



A robust fuzzy control approach for path-following control of autonomous vehicles

Ardashir Mohammadzadeh¹ · Hamid Taghavifar²

Published online: 22 May 2019
© Springer-Verlag GmbH Germany, part of Springer Nature 2019

Abstract

This paper presents a robust fuzzy control approach for the lateral path-following of autonomous road vehicles (ARVs). The dynamics of the ARV is estimated online thorough a new non-singleton fuzzy system based on the non-stationary fuzzy sets. The asymptotic stability of the proposed method is ensured, and the adaptation laws for the proposed fuzzy system are derived based on the Lyapunov stability theorem. The robustness of the proposed control method is verified for a vehicle system performing a double-lane-change maneuver at different forward speeds subjected to structured and unmodeled uncertainties and different disturbances. The effectiveness of the proposed approach is further investigated under different measurement noise levels. Based on the obtained results, it is concluded that the proposed control strategy can be effectively applied to the path-following task of ARVs under a wide range of operating conditions and external disturbances.

Keywords Fuzzy system · Non-stationary fuzzy sets · Compensator · Robustness · Autonomous vehicles

1 Introduction

The emerging progress in cyber-physical systems, advanced control paradigms and deployment of artificial intelligence techniques have strongly assisted to address the long-term demands of human driver safety, ease of ride, accident avoidance, energy efficiency, road utilization and convenient trafficking through the application of the automated and connected vehicles, advanced driving assistance systems (ADAS) and parallel steering control (Guo et al. 2018; Hu et al. 2016). However, the sophisticated road conditions, modern urban infrastructure complexities and dynamic trafficking requirements impose the introduction of more effective and state-of-the-art control frameworks for autonomous road vehicles (ARVs) (González et al. 2016; Zhu et al. 2017). There is a broad range of operational objectives

related to the performance of ARVs. Lateral path-following and lane keeping criteria serve as the substantial motion control objectives for ARVs in order to ensure the vehicle security and the lateral motion stability (Naranjo et al. 2008; Wang et al. 2017). The controllers employed for lateral path-following of ARVs are typically the active front wheel steering (AFS), direct yaw moment control (DYC) or invariants of the coupled control paradigm. The integrated control schemas are suggestive of the improved vehicle handling and stability performance by employing AFS and DYC in a simultaneous manner. Therefore, path-following task can be also effectively achieved by employing the integrated control approach even at considerably higher speed limits because of the flexibility and availability of independently actuated controllers (Yim et al. 2016).

The path-following task of ARVs comprises the precise navigation of the target vehicle on a prescribed path, and this in turn causes significant difficulties. The navigation of ARVs is entirely performed without the driver intervention or any prior understanding of the desired trajectory in the time domain (Aguiar and Hespanha 2007). Additionally, the constraints on the vehicle states and the ambient vehicles, pedestrians and their unpredictable responses significantly increase the burdens of an effective controller design for ARVs. The minimal path-following errors are typically introduced in terms of the lateral offset and the heading error under

Communicated by V. Loia.

✉ Ardashir Mohammadzadeh
a.mzadeh@bonabu.ac.ir
Hamid Taghavifar
h_taghav@encs.concordia.ca

¹ Electrical Engineering Department, University of Bonab, Bonab, Iran

² Department of Mechanical and Industrial Engineering, Concordia University, Montreal, Canada

varying driving conditions (Hu et al. 2015, 2019; Hu 2016). Consequently, the primary goal in the design of control laws is regularly to push the lateral path-following error toward zero, while the vehicle stability is upheld during various maneuvering conditions. In the case of smooth trajectories with the known system dynamics, typically the invariants of feedback control laws can accomplish reasonably effective results (Li et al. 2017). Practically speaking, though, the desired trajectories are non-smooth paths and even fail to comply with the vehicle constraining kinematic or dynamics. In emergent scenarios and critical maneuvering conditions such as collision avoidance, a huge actuator input may be required in a short span of time. An improper feedback law can perhaps cause critical instability for highly curved paths or those maneuvers demanding swift yaw stabilization. Therefore, only those control schemas which address the optimality and robustness against the unknown dynamics of the system can potentially serve as a remedy to the practical setbacks related to the path-following of ARVs.

The archived reported studies are indicative of a broad class of control theories employing for the path-following of ARVs such as composite nonlinear feedback (Hu et al. 2016), adaptive neural network (Wai et al. 2010; Yang et al. 2013), genetic-based method (Shih et al. 2017), robust H_∞ output feedback control (Wang et al. 2016) and backstepping control method (Kang et al. 2018). The aforesaid approaches can typically enhance the effectiveness of the path-following performance of ARVs; however, most of them ignore the effect of unknown dynamics of the vehicle on the system response. Indeed, the controllers should be generic and expandable to any other vehicle system with slight variations and the control laws should not vary from one vehicle to another. For instance, MPC technique requires an explicit model of the system and the exact states of the system over the prediction horizon. However, the vehicle system is not deterministic and holds extensive amount structural and unmodeled uncertainties. For example, the tires are substantially subjected to saturation, and therefore, the lateral force can be insufficient for the vehicle handling. Therefore, the response of the tire in terms of the force deflection enters the hard non-linearity region. In response, though, the tires cornering force hardly varies or, at times, deteriorates with the development of sideslip angle and pushes the vehicle to the driving limits (Ji et al. 2018). In light of the arguments explored above, it is essential to examine the ways to diminish the unfavorable impact of the modeled or unmodeled uncertainties as well as the external disturbances on the lateral path-following of ARVs. The adaptive intelligent control schemes can potentially meet the requirement of desired control performance against the considerable system uncertainty by learning to approximate any arbitrary nonlinear and uncertain but bounded models (He et al. 2016; Ghaffari and Homaeinezhad 2018; Jeon et al. 2016).

The fuzzy systems are popular in control systems, fault detection systems and feature extraction methods (Deng et al. 2018; Zhao et al. 2016). The fuzzy systems have also been employed in path-following of autonomous robot vehicles (Saffiotti 1997), commercial vehicles (Rodríguez-Castaño et al. 2016) and ARVs (Zhang et al. 2019; Rastelli and Peñas 2015; Hwang et al. 2018). A T-S fuzzy model with the additional norm-bounded uncertainty-based controller was developed for vehicle path-following in the presence of non-linearities and parametric uncertainties related to the variations in vehicle mass and cruise control (Zhang et al. 2019). AFS was employed as the only controlling effort, and later, a method to the fuzzy observer-based output feedback AFS control for ARV was designed using the Lyapunov stability theorem. Another study was reported by employing a similar controlling strategy using AFS as the only control input (Rastelli and Peñas 2015). A fuzzy logic system for ARVs and the cascade structure for lateral path-following control and parametric trajectory for inside the roundabout were designed. The potential drawback for discussed papers is the presence of a single control input which can be simply saturated at driving limits and exhibit limited functionality. An integrated AFS and DYC method serves as a reasonable solution for heading angle and lateral offset error stabilization independently. Hwang et al. Hwang et al. (2018) employed a hierarchically improved fuzzy dynamical sliding mode control for the path-following purpose of ARVs, while the designed controller comprised of two stages: One was related to the virtual desired input and the other was the path-following control. The proposed hierarchical dynamic fuzzy sliding mode controller was designed to address the challenge related to the system uncertainties, particularly, varying payloads. The proposed controller realized a tuning mechanism to withstand the uncertainties related to the weight of the vehicle by the Lyapunov stability with the hierarchical concept with minimal computational demand.

The reviewed literature indicates that few studies have been reported on the adaptive robust fuzzy control, for the path-following task of ARVs considering the unmodeled and parametric uncertainties of the vehicles. According to the above motivations, a robust fuzzy control is proposed in this paper. The performance of the fuzzy controllers depends on the approximation capability of the fuzzy systems. To improve the estimation performance of the traditional fuzzy systems and to cope with the computational cost of the type 2 fuzzy systems, a new non-singleton fuzzy system based on the non-stationary fuzzy sets is proposed. To tune the parameters of the fuzzy systems in the control scheme many optimization methods can be used such as ant colony optimization (Deng et al. 2019), particle swarm optimization (Deng et al. 2019, 2017) and genetic algorithm (Deng et al. 2017). In this paper some adaptation laws are extracted

through the robustness analysis of the closed-loop system to optimize the fuzzy systems.

The most important advantages of the proposed control scheme are summarized as follows:

1. The proposed control scheme does not use the mathematical model of the vehicle. The dynamics are assumed to be unknown and are perturbed by some disturbances such as changing of the tire cornering stiffness.
2. The unknown and perturbed dynamics of the vehicle are estimated online using proposed non-singleton fuzzy systems based on the non-stationary fuzzy sets. Then the estimation ability of the traditional fuzzy systems is improved.
3. The robustness of control scheme against the measurement errors is taken to account.
4. The robustness of the proposed control method against external disturbances and different longitudinal velocities is guaranteed by the proposed new adaptive compensator.

The remainder of the paper is organized as follows. In Sect. 2, the ARV dynamic model is formulated to follow a desired path trajectory. The proposed fuzzy system is illustrated in Sect. 3. In Sect. 4, the robust fuzzy control theory is developed. The simulations and results are provided in Sect. 5, and the conclusions are outlined in Sect. 6.

2 Problem formulation

Typically, the contribution of longitudinal forces applied to the vehicle such as rolling resistance and traction force developed at the tire-ground interface is assumed infinitesimal on the cornering response of the vehicle. However, the forward vehicle speed has to be sufficient for generating the lateral forces proportional to the slip angles. In this study, a two-degree-of-freedom (2-DOF) bicycle model is considered (Fig. 1) due to the symmetric dynamics of the right and left tracks of the vehicle. The major goal of yaw angle or heading angle control system is to prevent vehicles from rotating and losing yaw stability and to keep the yaw velocity as close as possible to the nominal value anticipated from an expert driver. Hence, the yaw angle is desired to remain at a slight magnitude range. For the path-following as indicated in Fig. 1, the lateral offset error indicates the closest distance between the vehicle and the desired trajectory as an orthogonal projection. Furthermore, the yaw rate γ is defined as the derivative of the vehicle heading angle. The difference between the vehicle yaw rate and the desired one γ_d is representative of the yaw rate error γ_e which is further denoted by the derivatives of the vehicle heading angle φ and the desired heading angle. The path-following errors can be therefore

determined as:

$$\begin{cases} \gamma_e = \gamma - \gamma_d = \gamma - v_x/R(\rho) \\ \dot{\gamma} = v_x \sin \varphi + v_y \cos \varphi \\ \dot{\varphi} = \gamma \end{cases} \quad (1)$$

where $R(\rho)$ is the radius of curvature of the desired path at the point shown in Fig. 1 and ρ represents the arc length of the represented point which changes by the trajectory of the road; the curvature will change accordingly. The purpose is indeed to devise a robust controller to globally asymptotically converge the terms γ_e and $\dot{\gamma}$ to zero. Consequently, the vehicle can follow the desired trajectory after stabilization. Regarding the governing equations of the motion, it is noteworthy that due to the infinitesimal contribution of the pitch and roll motions to the path-following of the vehicle in yaw plane, these terms are dismissed in the model. Furthermore, the front steering is considered in the model as the control input since the external yaw moment generation has limited application in real tests where a robust steering controller is sufficient in practical experiments (Fang et al. 2011). The 2-DOF yaw plane vehicle model can be simply expressed as:

$$\begin{cases} \dot{v}_y = \frac{1}{m} (F_{yf} + F_{yr}) - v_x \gamma \\ \dot{\gamma} = \frac{1}{I_z} (F_{yf}l_f - F_{yr}l_r + \Delta T) \end{cases} \quad (2)$$

where v_x and v_y are the longitudinal and lateral velocities in the body-fixed coordinate y and \dot{y} represent the lateral displacement and velocity of the vehicle center of gravity (C.G.), φ and $\dot{\varphi}$ denote the vehicle heading angle and yaw rate, ΔT is the external yaw moment, F_{yf} and F_{yr} are the lateral tire force related to the front and rear wheels, l_f and l_r are the distance between the (C.G.) and front and rear wheels, respectively, m is the vehicle mass and I_z is the mass moment of inertia about the yaw axis. The external yaw moment applied to the vehicle with track width l_b can be expressed as:

$$\Delta T = \sum_i \sum_{j=1}^2 (-1)^j F_{xij} \frac{l_b}{2} \quad i = f, r \quad (3)$$

Considering the aforesaid proportionality between the tire lateral force and the sideslip angles, the lateral forces are simply presented as a function of the front and rear tire cornering stiffness parameters (i.e., C_f and C_r) as follows.

$$F_{yf} = C_f \alpha_f, \quad F_{yr} = C_r \alpha_r \quad (4)$$

Aiming to consider the nonlinear cornering characteristics of tire, the role of uncertainty can be included as:

$$C_f = \tilde{C}_f + \Delta C_f, \quad C_r = \tilde{C}_r + \Delta C_r \quad (5)$$

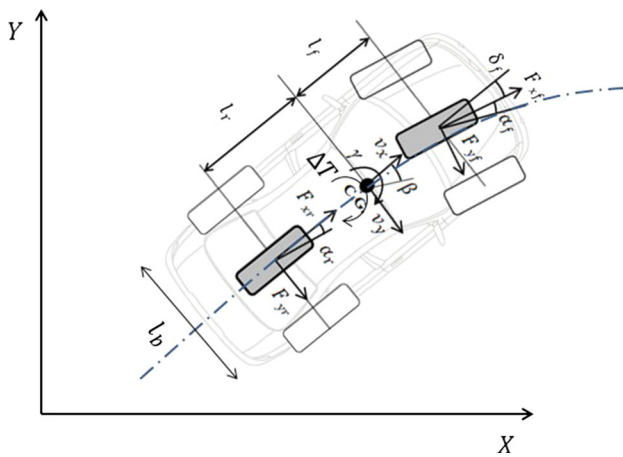


Fig. 1 Schematic representation of an autonomous vehicle yaw plane model and the path-following maneuver

where \tilde{C}_f and \tilde{C}_r denote for the nominal cornering stiffness for the front and rear tires, respectively, limited to the linear region of tire deformation, and ΔC_f and ΔC_r represent the bounded uncertainties for tire cornering stiffness of front and rear wheels, respectively. Furthermore, the sideslip angles related to the front and rear tires can be represented as:

$$\begin{cases} \alpha_f = \tan^{-1} \left[\frac{v_x \sin(\beta) + l_f \gamma}{v_x \cos(\beta)} \right] - \delta_f \\ \alpha_r = \tan^{-1} \left[\frac{v_x \sin(\beta) - l_r \gamma}{v_x \cos(\beta)} \right] \end{cases} \quad (6)$$

where δ_f and β represent the front wheel steering angle and sideslip angle ($\beta \approx v_y/v_x$). By substituting (3)–(6), in (2) and (1), the following can be derived:

$$\begin{cases} \dot{y} = v_x \sin \varphi + v_y \cos \varphi \\ \dot{v}_y = \frac{C_f}{m} \left\{ \tan^{-1} \left[\frac{v_x \sin(\beta) + l_f \gamma}{v_x \cos(\beta)} \right] - \delta_f \right\} \\ \quad + \frac{C_r}{m} \left\{ \tan^{-1} \left[\frac{v_x \sin(\beta) - l_r \gamma}{v_x \cos(\beta)} \right] \right\} - v_x \gamma \\ \dot{\gamma} = \frac{1}{I_z} \left(\left\{ l_f C_f \tan^{-1} \left[\frac{v_x \sin(\beta) + l_f \gamma}{v_x \cos(\beta)} \right] - \delta_f \right\} \right. \\ \quad \left. + \left\{ l_r C_r \tan^{-1} \left[\frac{v_x \sin(\beta) - l_r \gamma}{v_x \cos(\beta)} \right] \right\} + \Delta T \right) \end{cases} \quad (7)$$

The dynamics of the system are rewritten as follows:

$$\begin{aligned} \dot{x}_1 &= f_1(\underline{x}) + b_1 u_1 \\ \dot{x}_2 &= f_2(\underline{x}) + b_2 u_2 \end{aligned} \quad (8)$$

where $x_1 = v_y$, $x_2 = \gamma$, $u_1 = \delta_f$, $u_2 = \Delta T$, $b_1 = \frac{1}{I_z}$, $b_2 = \frac{C_f}{m}$ and

$$\begin{aligned} f_1(\underline{x}) &= \frac{C_f}{m} \left\{ \tan^{-1} \left[\frac{v_x \sin(\beta) + l_f \gamma}{v_x \cos(\beta)} \right] \right\} \\ &\quad + \frac{C_r}{m} \left\{ \tan^{-1} \left[\frac{v_x \sin(\beta) - l_r \gamma}{v_x \cos(\beta)} \right] \right\} - v_x \gamma \end{aligned} \quad (9)$$

$$\begin{aligned} f_2(\underline{x}) &= \frac{1}{I_z} \left\{ l_f C_f \tan^{-1} \left[\frac{v_x \sin(\beta) + l_f \gamma}{v_x \cos(\beta)} \right] - \delta_f \right\} \\ &\quad + \left\{ l_r C_r \tan^{-1} \left[\frac{v_x \sin(\beta) - l_r \gamma}{v_x \cos(\beta)} \right] \right\} \end{aligned} \quad (10)$$

The general view on the proposed control scheme is shown in Fig. 2. The details are described below.

3 Proposed non-singleton fuzzy system based on non-stationary fuzzy sets

As mentioned before, the dynamics of the vehicle are assumed to be unknown and are estimated online. It has been shown that the approximation capability of the type 2 fuzzy systems is more than type 1 counterpart and the type 2 fuzzy systems result in good performance in contrast to type 1 fuzzy systems. But computational cost of type 2 fuzzy systems is significantly more than type 1 counterpart (Castillo et al. 2011). To improve the estimation performance of the traditional fuzzy systems and to cope with the computational cost of the type 2 fuzzy systems, a new non-singleton fuzzy system based on the non-stationary fuzzy sets is proposed. A non-stationary fuzzy set is defined as follows (Garibaldi et al. 2008):

$$A = \int_{x \in X} \int_{t \in T} \mu_A(t, x) / x / t \quad (11)$$

where $(t, x) \in T \times X$, $T \times X \rightarrow [0, 1]$ and $\mu_A(t, x)$ is expressed as $\mu_A(t, x) = \mu_A(x, p_1(t), \dots, p_m(t))$, in which $p_i(t) = p_i + k_i f_i(t)$, $i = 1, \dots, m$ and $f_i(t)$ is a perturbation function. In this paper by using the concept of non-stationary fuzzy sets, a non-singleton fuzzy system is proposed for estimation of uncertainties. The structure of the proposed fuzzy system is shown in Fig. 3.

The output of the fuzzy system is obtained step by step as follows:

- (1) *Input layer* Get the input $x = [x_1, \dots, x_n]^T$.
- (2) *Fuzzification layer* Apply non-singleton fuzzification by considering a fuzzy set for each input as follows:

$$\begin{aligned} \mu_{B_i}(x_i) &= \exp \left(- \frac{(x_i - x'_i)^2}{\sigma_x^2} \right) \\ i &= 1, \dots, n \end{aligned} \quad (12)$$

where x'_i is the value of input x_i and σ_x is a constant parameter which represents the level of input uncertainty.

Fig. 2 Block diagram of the proposed control scheme

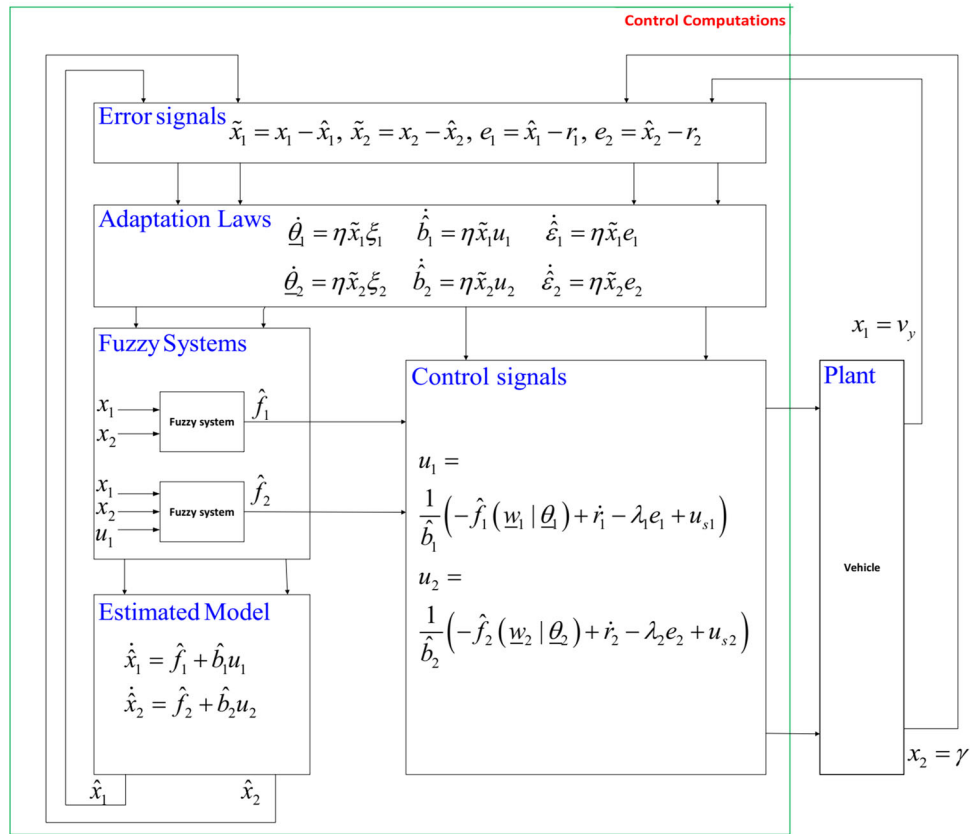
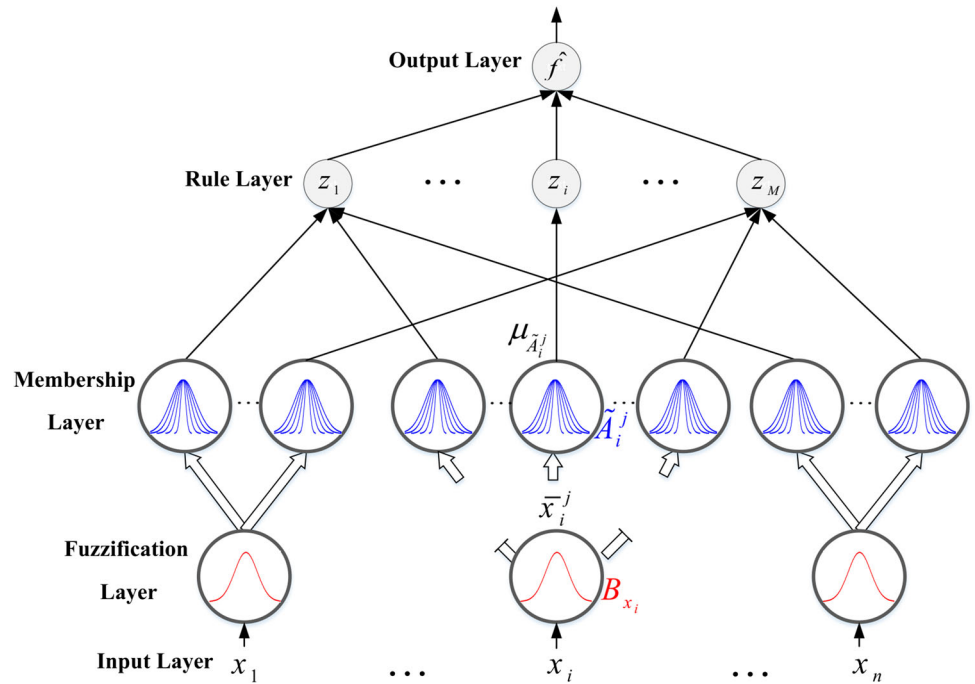


Fig. 3 Proposed fuzzy system



- (3) *Membership layer* Compute the memberships of all MF for each input as follows:

$$\mu_{\tilde{A}_i^j}(x_i) = \frac{1}{K} \sum_{k=1}^K xp \left(-\frac{(\bar{x}_i(k) - c_{\tilde{A}_i^j})^2}{\sigma_{\tilde{A}_i^j}^2(k)} \right) \quad (13)$$

$$i = 1, \dots, n \quad j = 1, \dots, M$$

where \tilde{A}_i^j represent the j th non-stationary MF for i th input. The center of \tilde{A}_i^j is $c_{\tilde{A}_i^j}$ and its width is changed between $\sigma_{\tilde{A}_i^j}^2(1)$ and $\sigma_{\tilde{A}_i^j}^2(K)$. K is the number of embedded MFs (see Fig. 4). M is the number of MFs for each input, n is the number of inputs and $\bar{x}_i(k)$ is obtained based on minimum t-norm inference as follows:

$$\bar{x}_i(k) = \frac{\sigma_x^2 c_{\tilde{A}_i^j} + \sigma_{\tilde{A}_i^j}^2(k) x'_i(k)}{\sigma_x^2 + \sigma_{\tilde{A}_i^j}^2(k)} \quad (14)$$

- (4) *Rule layer* Consider the rules as follows:

$$\begin{aligned} & \text{if } x_1 \text{ is } A_1^l \text{ and } \dots \text{ and } x_i \text{ is } A_i^l \\ & \text{and } \dots \text{ and } x_n \text{ is } A_n^l \text{ then } y \text{ is } \theta_l \\ & l = 1, \dots, M \end{aligned} \quad (15)$$

where M is the number of rules, A_1^l is the l th MF for i th input and θ_l is the l th consequent parameter. Then the degrees of rule firing are computed as follows:

$$z_l = \prod_{i=1}^n \mu_{A_i^l}, \quad l = 1, \dots, M \quad (16)$$

where z_l represent the firing degree of l th rule.

- (5) *Output layer* The output of the fuzzy system is obtained as follows:

$$\hat{f} = \frac{\sum_{l=1}^M z_l \theta_l}{\sum_{l=1}^M z_l} \quad (17)$$

The fuzzy system can be written as the following vector form:

$$\hat{f} = \underline{\theta}^T \xi \quad (18)$$

where

$$\begin{aligned} \underline{\theta} &= [\theta_1, \dots, \theta_M]^T \\ \xi &= [\xi_1, \dots, \xi_M]^T \\ \xi_l &= \frac{z_l}{\sum_{l=1}^M z_l} \end{aligned} \quad (19)$$

4 Control design and stability analysis

The dynamics of the system in (8) are estimated as follows:

$$\begin{aligned} \dot{\hat{x}}_1 &= \hat{f}_1(\underline{w}_1 | \underline{\theta}_1) + \hat{b}_1 u_1 \\ \dot{\hat{x}}_2 &= \hat{f}_2(\underline{w}_2 | \underline{\theta}_2) + \hat{b}_2 u_2 \end{aligned} \quad (20)$$

where \hat{x}_1 and \hat{x}_2 are the estimations of x_1 and x_2 , respectively. \hat{f}_1 and \hat{f}_2 are the proposed T2FNN, which estimate the uncertainties and disturbances. \hat{b}_1 and \hat{b}_2 are the estimations of control gains b_1 and b_2 , respectively. u_1 and u_2 are control signals, and $\underline{\theta}_1$ and $\underline{\theta}_2$ are the trainable parameters of \hat{f}_1 and \hat{f}_2 , respectively. \underline{w}_1 and \underline{w}_2 are the input variables of \hat{f}_1 and \hat{f}_2 , respectively, which are considered as follows:

$$\begin{aligned} \underline{w}_1 &= [x_1, x_2]^T \\ \underline{w}_2 &= [x_1, x_2, u_1]^T \end{aligned} \quad (21)$$

Then by considering (8) and (20), the dynamics of the estimation errors $\tilde{x}_1 = x_1 - \hat{x}_1$ and $\tilde{x}_2 = x_2 - \hat{x}_2$ are obtained as follows:

$$\begin{aligned} \dot{\tilde{x}}_1 &= f_1(\underline{x}) - \hat{f}_1(\underline{w}_1 | \underline{\theta}_1) + (b_1 - \hat{b}_1) u_1 \\ \dot{\tilde{x}}_2 &= f_2(\underline{x}) - \hat{f}_2(\underline{w}_2 | \underline{\theta}_2) + (b_2 - \hat{b}_2) u_2 \end{aligned} \quad (22)$$

By defining the optimal values of the parameters $\underline{\theta}_i, i = 1, 2$ as $\underline{\theta}_i^*$, the dynamics of \tilde{x}_1 and \tilde{x}_2 in (22), are rewritten as follows:

$$\begin{aligned} \dot{\tilde{x}}_1 &= \hat{f}_1(\underline{w}_1 | \underline{\theta}_1^*) - \hat{f}_1(\underline{w}_1 | \underline{\theta}_1) \\ & \quad + f_1(\underline{x}) - \hat{f}_1(\underline{w}_1 | \underline{\theta}_1^*) + (b_1 - \hat{b}_1) u_1 \\ \dot{\tilde{x}}_2 &= \hat{f}_2(\underline{w}_2 | \underline{\theta}_2^*) - \hat{f}_2(\underline{w}_2 | \underline{\theta}_2) \\ & \quad + f_2(\underline{x}) - \hat{f}_2(\underline{w}_2 | \underline{\theta}_2^*) + (b_2 - \hat{b}_2) u_2 \end{aligned} \quad (23)$$

The approximation errors are defined as follows:

$$\begin{aligned} E_1 &= f_1(\underline{x}) - \hat{f}_1(\underline{w}_1 | \underline{\theta}_1^*) \\ E_2 &= f_2(\underline{x}) - \hat{f}_2(\underline{w}_2 | \underline{\theta}_2^*) \end{aligned} \quad (24)$$

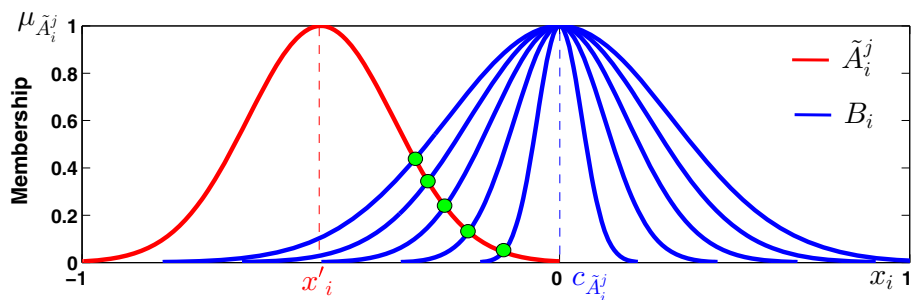
From (24) and the vector form of fuzzy system (18), equation (23) is rewritten as follows:

$$\begin{aligned} \dot{\tilde{x}}_1 &= \tilde{\underline{\theta}}_1^T \xi_1 + E_1 + (b_1 - \hat{b}_1) u_1 \\ \dot{\tilde{x}}_2 &= \tilde{\underline{\theta}}_2^T \xi_2 + E_2 + (b_2 - \hat{b}_2) u_2 \end{aligned} \quad (25)$$

where $\tilde{\underline{\theta}}_i = \underline{\theta}_i^* - \underline{\theta}_i, i = 1, 2$.

Remark 1 The approximation errors E_1 and E_2 are written as $E_1 = \varepsilon_1 e_1$ and $E_2 = \varepsilon_2 e_2$, respectively, in which ε_1 and ε_2 are estimated as $\hat{\varepsilon}_1$ and $\hat{\varepsilon}_2$, respectively.

Fig. 4 Non-singleton fuzzification



Theorem 1 System (8) is asymptotically stable if the control signals and adaptation laws are chosen as follows:

$$\begin{aligned}
 u_{s1} &= \frac{1}{\hat{b}_1} \left(-\hat{f}_1(\underline{w}_1|\underline{\theta}_1) + \dot{r}_1 - \lambda_1 e_1 + u_{s1} \right) \\
 u_{s2} &= \frac{1}{\hat{b}_2} \left(-\hat{f}_2(\underline{w}_2|\underline{\theta}_2) + \dot{r}_2 - \lambda_2 e_2 + u_{s2} \right)
 \end{aligned} \tag{26}$$

$$\begin{aligned}
 u_{s1} &= -\tilde{x}_1 \hat{e}_1 \\
 u_{s2} &= -\tilde{x}_2 \hat{e}_2
 \end{aligned} \tag{27}$$

$$\begin{aligned}
 \dot{\underline{\theta}}_1 &= \eta \tilde{x}_1 \xi_1 \\
 \dot{\underline{\theta}}_2 &= \eta \tilde{x}_2 \xi_2
 \end{aligned} \tag{28}$$

$$\begin{aligned}
 \dot{\hat{b}}_1 &= \eta \tilde{x}_1 u_1 \\
 \dot{\hat{b}}_2 &= \eta \tilde{x}_2 u_2
 \end{aligned} \tag{29}$$

$$\begin{aligned}
 \dot{\hat{\varepsilon}}_1 &= \eta \tilde{x}_1 e_1 \\
 \dot{\hat{\varepsilon}}_2 &= \eta \tilde{x}_2 e_2
 \end{aligned} \tag{30}$$

where r_1 and r_2 are the reference signals. λ_1 and λ_2 are positive constants. u_{s1} and u_{s2} are compensators. e_1 and e_2 are tracking errors, which are defined as $e_1 = \hat{x}_1 - r_1$ and $e_2 = \hat{x}_2 - r_2$, $\tilde{x}_1 = x_1 - \hat{x}_1$, $\tilde{x}_2 = x_2 - \hat{x}_2$ and η is the adaptation rate.

From (20) and (26), the dynamics of the tracking errors are obtained as follows:

$$\begin{aligned}
 \dot{e}_1 &= -\lambda_1 e_1 + u_{s1} \\
 \dot{e}_2 &= -\lambda_2 e_2 + u_{s2}
 \end{aligned} \tag{31}$$

For the aim of stability analysis, the following Lyapunov function is considered:

$$\begin{aligned}
 V &= \frac{1}{2} e_1^2 + \frac{1}{2} e_2^2 + \frac{1}{2} \tilde{x}_1^2 + \frac{1}{2} \tilde{x}_2^2 \\
 &+ \frac{1}{2\eta} \tilde{\theta}_1^T \tilde{\theta}_1 + \frac{1}{2\eta} \tilde{\theta}_2^T \tilde{\theta}_2 \\
 &+ \frac{1}{2\eta} \tilde{\varepsilon}_1^2 + \frac{1}{2\eta} \tilde{\varepsilon}_2^2 + \frac{1}{2\eta} \tilde{b}_1^2 + \frac{1}{2\eta} \tilde{b}_2^2
 \end{aligned} \tag{32}$$

where $e_i = \hat{x}_i - r_i$, $\tilde{x}_i = x_i - \hat{x}_i$, $\tilde{\theta}_i = \underline{\theta}_i^* - \underline{\theta}_i$, $\tilde{\varepsilon}_i = \varepsilon_i - \hat{\varepsilon}_i$, $\tilde{b}_i = b_i - \hat{b}_i$, $i = 1, 2$ and η is the adaptation rate.

Time derivative of V in (32) yields:

$$\begin{aligned}
 \dot{V} &= e_1 \dot{e}_1 + e_2 \dot{e}_2 + \tilde{x}_1 \dot{\tilde{x}}_1 + \tilde{x}_2 \dot{\tilde{x}}_2 \\
 &- \frac{1}{\eta} \tilde{\theta}_1^T \dot{\tilde{\theta}}_1 - \frac{1}{\eta} \tilde{\theta}_2^T \dot{\tilde{\theta}}_2 \\
 &- \frac{1}{\eta} \tilde{\varepsilon}_1 \dot{\tilde{\varepsilon}}_1 - \frac{1}{\eta} \tilde{\varepsilon}_2 \dot{\tilde{\varepsilon}}_2 - \frac{1}{\eta} \tilde{b}_1 \dot{\tilde{b}}_1 - \frac{1}{\eta} \tilde{b}_2 \dot{\tilde{b}}_2
 \end{aligned} \tag{33}$$

By substituting \dot{e}_i and $\dot{\tilde{x}}_i$, $i = 1, 2$, from (25) and (31), into (33), \dot{V} becomes:

$$\begin{aligned}
 \dot{V} &= e_1 (-\lambda_1 e_1 + u_{s1}) + e_2 (-\lambda_2 e_2 + u_{s2}) \\
 &+ \tilde{x}_1 \left(\tilde{\theta}_1^T \xi_1 + E_1 + \tilde{b}_1 u_1 \right) + \tilde{x}_2 \left(\tilde{\theta}_2^T \xi_2 + E_2 + \tilde{b}_2 u_2 \right) \\
 &- \frac{1}{\eta} \tilde{\theta}_1^T \dot{\tilde{\theta}}_1 - \frac{1}{\eta} \tilde{\theta}_2^T \dot{\tilde{\theta}}_2 \\
 &- \frac{1}{\eta} \tilde{\varepsilon}_1 \dot{\tilde{\varepsilon}}_1 - \frac{1}{\eta} \tilde{\varepsilon}_2 \dot{\tilde{\varepsilon}}_2 - \frac{1}{\eta} \tilde{b}_1 \dot{\tilde{b}}_1 - \frac{1}{\eta} \tilde{b}_2 \dot{\tilde{b}}_2
 \end{aligned} \tag{34}$$

By some simplifications, one obtains:

$$\begin{aligned}
 \dot{V} &= -\lambda_1 e_1^2 + e_1 u_{s1} - \lambda_2 e_2^2 + e_2 u_{s2} \\
 &+ \tilde{\theta}_1^T \left(\tilde{x}_1 \xi_1 - \frac{1}{\eta} \dot{\tilde{\theta}}_1 \right) + \tilde{x}_1 E_1 \\
 &+ \tilde{\theta}_2^T \left(\tilde{x}_2 \xi_2 - \frac{1}{\eta} \dot{\tilde{\theta}}_2 \right) + \tilde{x}_2 E_2 \\
 &\tilde{b}_1 \left(\tilde{x}_1 u_1 - \frac{1}{\eta} \dot{\tilde{b}}_1 \right) + \tilde{b}_2 \left(\tilde{x}_2 u_2 - \frac{1}{\eta} \dot{\tilde{b}}_2 \right) \\
 &- \frac{1}{\eta} \tilde{\varepsilon}_1 \dot{\tilde{\varepsilon}}_1 - \frac{1}{\eta} \tilde{\varepsilon}_2 \dot{\tilde{\varepsilon}}_2
 \end{aligned} \tag{35}$$

By choosing the adaptation laws as (28) and (29), \dot{V} becomes:

$$\begin{aligned}
 \dot{V} &= -\lambda_1 e_1^2 - \lambda_2 e_2^2 \\
 &+ \tilde{x}_1 E_1 + e_1 u_{s1} \\
 &+ \tilde{x}_2 E_2 + e_2 u_{s2} \\
 &- \frac{1}{\eta} \tilde{\varepsilon}_1 \dot{\tilde{\varepsilon}}_1 - \frac{1}{\eta} \tilde{\varepsilon}_2 \dot{\tilde{\varepsilon}}_2
 \end{aligned} \tag{36}$$

By adding and subtracting $\tilde{x}_i \hat{\varepsilon}_i e_i$ and replacing E_i as $E_i = \varepsilon_i e_i, i = 1, 2$, into (36), one obtains:

$$\begin{aligned} \dot{V} = & -\lambda_1 e_1^2 - \lambda_2 e_2^2 \\ & + \tilde{x}_1 \tilde{\varepsilon}_1 e_1 + e_1 u_{s1} + \tilde{x}_1 \hat{\varepsilon}_1 e_1 \\ & + \tilde{x}_2 \tilde{\varepsilon}_2 e_2 + e_2 u_{s2} + \tilde{x}_2 \hat{\varepsilon}_2 e_2 \\ & - \frac{1}{\eta} \tilde{\varepsilon}_1 \dot{\hat{\varepsilon}}_1 - \frac{1}{\eta} \tilde{\varepsilon}_2 \dot{\hat{\varepsilon}}_2 \end{aligned} \tag{37}$$

Equation (37) is simplified as follows:

$$\begin{aligned} \dot{V} = & -\lambda_1 e_1^2 - \lambda_2 e_2^2 \\ & + \tilde{\varepsilon}_1 \left(\tilde{x}_1 e_1 - \frac{1}{\eta} \dot{\hat{\varepsilon}}_1 \right) + e_1 u_{s1} + \tilde{x}_1 \hat{\varepsilon}_1 e_1 \\ & + \tilde{\varepsilon}_2 \left(\tilde{x}_2 e_2 - \frac{1}{\eta} \dot{\hat{\varepsilon}}_2 \right) + e_2 u_{s2} + \tilde{x}_2 \hat{\varepsilon}_2 e_2 \end{aligned} \tag{38}$$

Then by choosing adaptation laws as $\dot{\hat{\varepsilon}}_1 = \eta \tilde{x}_1 e_1$ and $\dot{\hat{\varepsilon}}_2 = \eta \tilde{x}_2 e_2$, it can be expressed that:

$$\begin{aligned} \dot{V} = & -\lambda_1 e_1^2 - \lambda_2 e_2^2 \\ & + e_1 u_{s1} + \tilde{x}_1 \hat{\varepsilon}_1 e_1 \\ & + e_2 u_{s2} + \tilde{x}_2 \hat{\varepsilon}_2 e_2 \end{aligned} \tag{39}$$

Then if u_{s1} and u_{s2} are chosen as $u_{s1} = -\tilde{x}_1 \hat{\varepsilon}_1$ and $u_{s2} = -\tilde{x}_2 \hat{\varepsilon}_2$, respectively, \dot{V} becomes:

$$\dot{V} = -\lambda_1 e_1^2 - \lambda_2 e_2^2 \tag{40}$$

To show that $\lim_{t \rightarrow \infty} e_1(t) \rightarrow 0$ and $\lim_{t \rightarrow \infty} e_2(t) \rightarrow 0$, the Barbalat’s lemma is used. Then it must be shown that $e_1 \in \ell^2$ and $e_2 \in \ell^2$. From (40), one has:

$$\begin{aligned} - \int_0^t \dot{V}(v) dv & = V(0) - V(t) \\ & \leq V(0) < \infty \end{aligned} \tag{41}$$

From (41), it is concluded that:

$$\lambda_1 \int_0^t e_1^2(v) dv + \lambda_2 \int_0^t e_2^2(v) dv < \infty \tag{42}$$

and

$$\begin{aligned} \int_0^t e_1^2(v) dv & < \infty \\ \int_0^t e_2^2(v) dv & < \infty \end{aligned} \tag{43}$$

Then, $e_1 \in \ell^2$ and $e_2 \in \ell^2$ and the asymptotically stability is derived.

Table 1 Simulation parameters

Parameter	Value	Unit
m	1480	kg
I_z	2350	kg m ²
l_f	1.05	m
l_r	1.63	m
C_f	67,500	N/rad
C_r	47,500	N/rad

5 Simulations

In this section, the effectiveness of the proposed method is examined by simulations for a typical road vehicle where the parameters employed in the study are specified in Table 1. Throughout the simulations, it is assumed that the vehicle travels on a dry asphalt road where the tire–road adhesion coefficient is sufficient to avoid the vehicle from lateral slide motion. The primary goal of the proposed controller is to push the autonomous vehicle to follow the desired path by minimizing the vehicle lateral offset and heading angle errors with a guaranteed stability. It is assumed to be constant and the reference trajectories are given as follows (Falcone et al. 2007):

$$\begin{aligned} r_1 & = \frac{d}{dt} \tan^{-1} \left\{ 4.05 \left(\frac{1}{\cos h(\bar{p})} \right)^2 \frac{1.2}{25} \right. \\ & \quad \left. - 5.7 \left(\frac{1}{\cos h(\bar{q})} \right)^2 \left(\frac{1.2}{21.95} \right) \right\} \\ r_2 & = \frac{d}{dt} \left\{ \frac{4.02}{2} (1 + \tanh(\bar{p})) - \frac{5.7}{2} (1 + \tanh(\bar{q})) \right\} \end{aligned} \tag{44}$$

where $\bar{p} = 2.4(vt - 27.19)/25 - 1.2$ and $\bar{q} = 2.4(vt - 56.46)/21.95 - 1.2$.

The longitudinal velocity is $v = 10$ m/s.

The trajectories of the lateral displacement and heading angle of the autonomous vehicle following the desired trajectories are illustrated in Fig. 5. It is evident that the vehicle holds the capacity to reach the desired trajectories very swiftly and keeps the track of them during the entire range of the simulation. The coupled effect of the vehicle yaw angle on the lateral displacement is suggestive of the reasonably considerable performance of the vehicle to follow the prescribed path because the vehicle yaw angle can be directly adjusted by an auxiliary control input (i.e., the direct yaw moment). Figure 5 shows that vehicle heading angle starts to vary from near $t = 3$ s until about $t = 9$ s, the range which the two lane changes occur successively and the lateral displacement trajectory exhibits a conforming response. The corresponding tracking errors are also presented in Fig. 6. It can be seen that the greatest lateral offset error is in the order of 0.06 m near $t = 5$ s which is related to the second lane-

Fig. 5 Lateral displacement and yaw angle

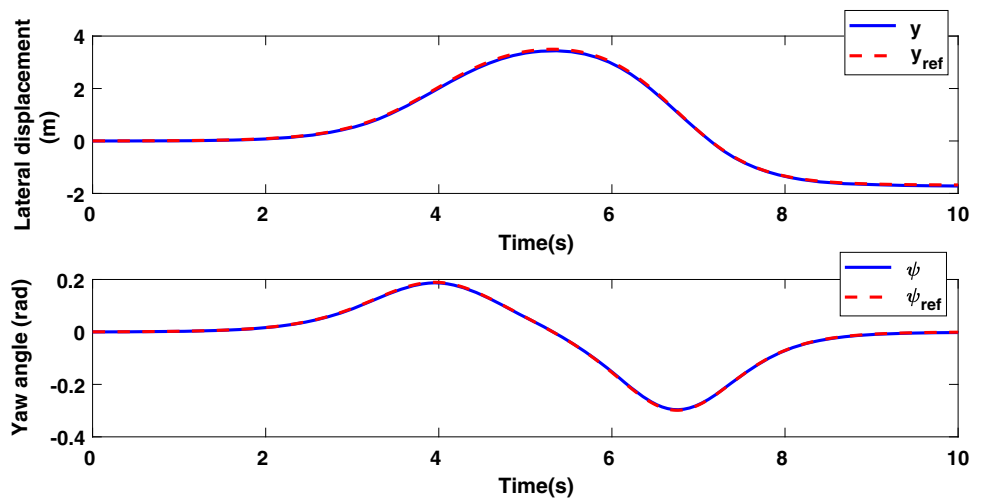


Fig. 6 Tracking error for lateral displacement and yaw angle

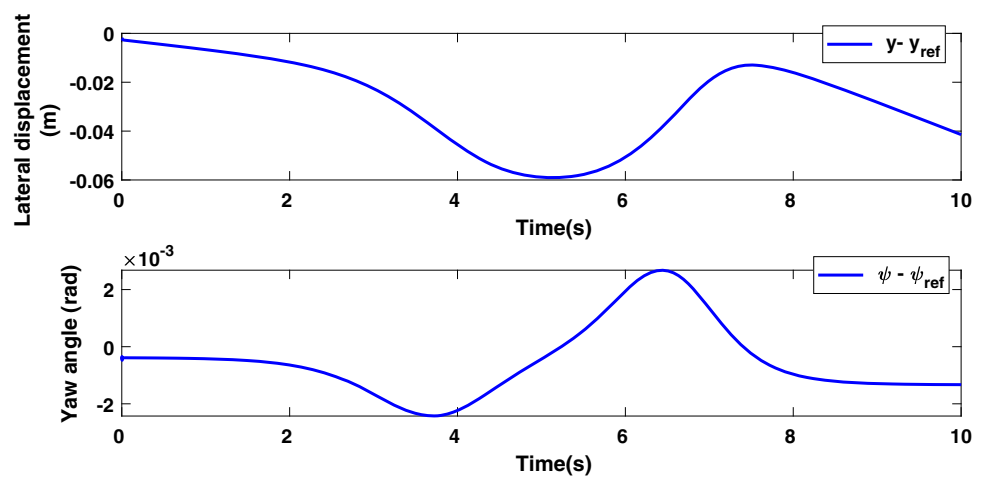


Fig. 7 Control signals

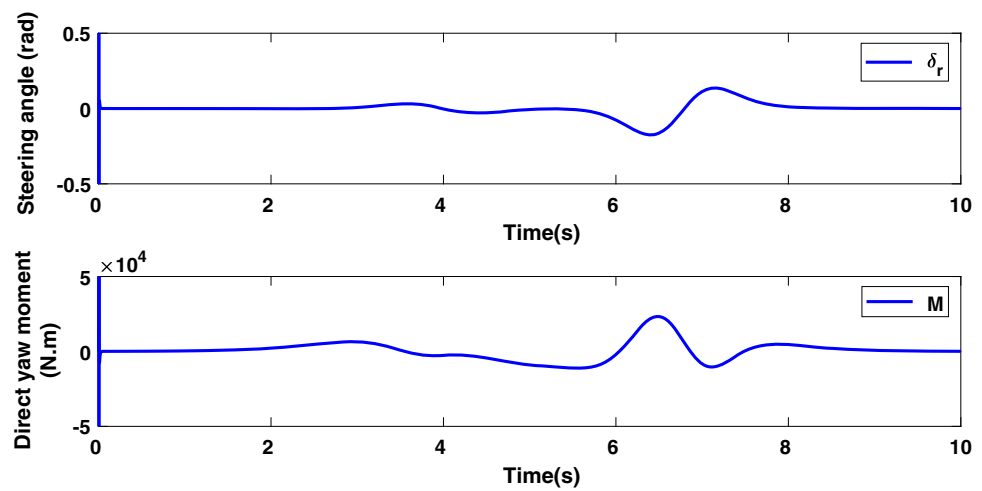


Table 2 Comparison of RMS and maximum values of tracking error for different control methods

	ADRC (Xia et al. 2016)	LQT (Xia et al. 2016)	Proposed method
y	0.2207	1.1049	0.0268
$\max(e_y)$	0.5592	1.7757	0.0451
ψ	0.0178	0.0592	0.0014
$\max(e_\psi)$	0.0363	0.1456	0.0017

Fig. 8 Lateral displacement and yaw angle, when the longitudinal velocity is 20 m/s

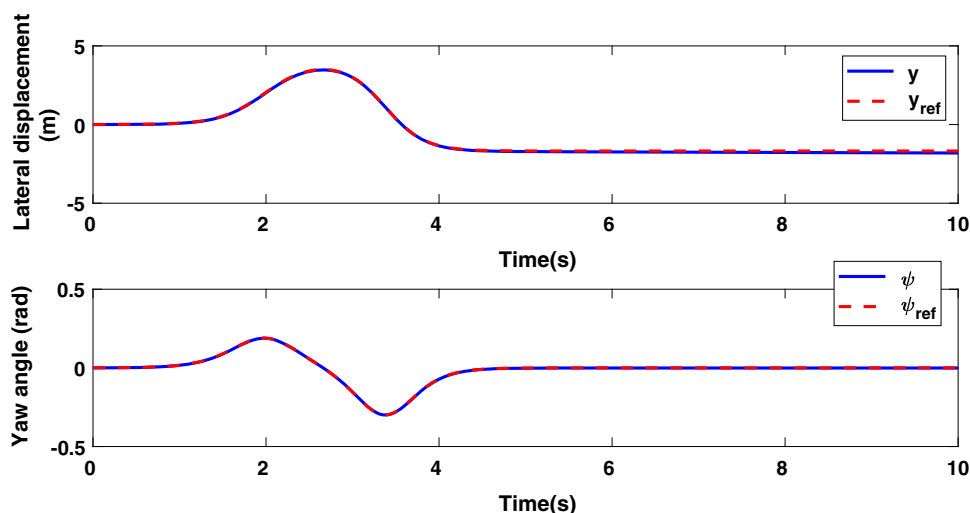
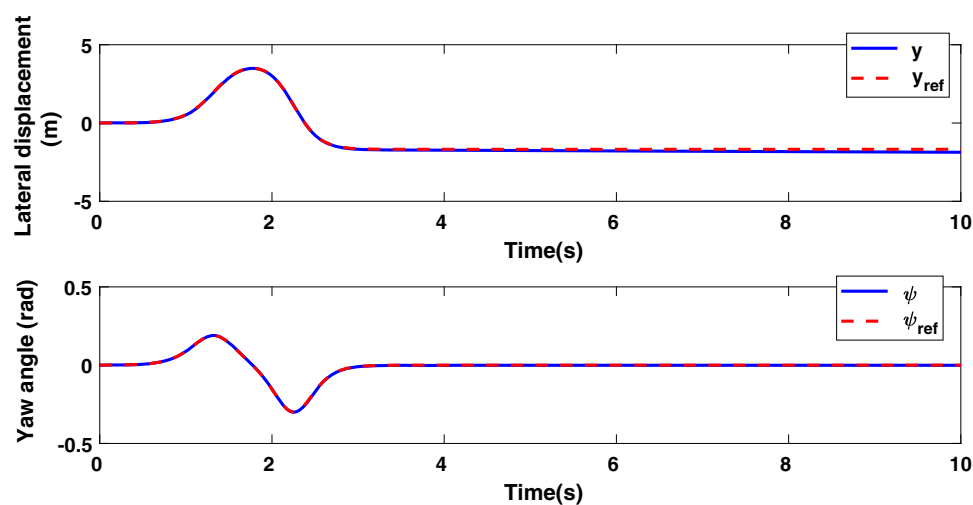


Fig. 9 Lateral displacement and yaw angle, when the longitudinal velocity is 30 m/s



change onset. The peak lateral offset error is attributed to the effect of inertial forces for an abrupt lateral force change direction. The heading angle error also lies within the small range ± 0.005 rad which ensures the vehicle path-following stability. The control signals related to the proposed method are also illustrated in Fig. 7 for the path-following control of the autonomous vehicle at nominal operating condition without disturbance. It is seen that the greatest AFS input occurs at the onset of the motion with a peak-to-peak magnitude of about 1 rad and then a quick stabilization of the controller signal. A similar trend is also observed for the DYC input where the peak magnitude approaches to 5000 N.m at the onset of simulation, followed by a quick attenuation of the control demand. The peak magnitude at the start of the motion is partly due to the time needed for the training of proposed FS adaptation laws, and the very swift stabilization of the controller inputs can be due to employing non-stationary fuzzy sets in the proposed method. The performance of the proposed control method is compared with the linear quadratic tracker (LQT) and active disturbance rejection

control (ADRC) method (Xia et al. 2016) in terms of the RMS and maximum values of tracking errors (Table 2). According to the performance measures, it is observed that the proposed controller outperforms the benchmarking methods. To show the robustness of the proposed control method, the simulations are further carried out under different longitudinal velocities, external disturbances and measurement errors.

5.1 Robustness against different longitudinal velocities

Forward speed of vehicle plays a significant role in the lateral stability of the vehicle through the coupled motion, which is demonstrated in terms of generating centrifugal acceleration. Hence, the tracking performance of the autonomous vehicle is further evaluated under an increased speed of 20 m/s and 30 m/s. The results related to the increased vehicle speed are illustrated in Figs. 8 and 9, respectively. The course of the same double-lane-change maneuver, therefore, is completed

Table 3 Comparison of RMS and maximum values of tracking error for different longitude velocities

	10 m/s	20 m/s	30 m/s
y	0.0268	0.0638	0.0963
$\max(e_y)$	0.0451	0.1198	0.1718
ψ	$9.6829e-4$	$7.8903e-4$	$8.4453e-4$
$\max(e_\psi)$	0.0017	0.0018	0.0030

within shorter simulation time in compliance with the forward speed. The values of RMS and maximum of tracking errors for different velocities are given in Table 3. As it can be seen, the variations in longitudinal velocity do not show significant effect on the tracking performance although the lane-change maneuvers have to be performed more abruptly. Table 3 shows further suggestive of the increase in the RMS and maximum values of tracking errors in terms of the lateral offset and heading angle under different longitudinal velocities. Such a trend can be also further confirmed according to Figs. 8 and 9. However, the increased errors related to the variations in the forward speed are in a reasonably small range and the ARV can keep the track of the desired path during the entire simulation period.

5.2 robustness against external disturbances

Although vehicle forward speed serves as a substantial source of uncertainty affecting the lateral force variations, there are other significant uncertainty and disturbances applied to the vehicle. According to (4), the nominal cornering stiffness for the front and rear tires can be varied to exceed the linearity region, and therefore, the lateral force saturation occurs. Furthermore, the role of different road–tire adhesion related to a low-adhesive icy road or high-adhesive dry asphalt can be consisted by the uncertainty term incorporated in the model based on (4). The different external disturbances are given in Table 4. For the first uncertainty case, the nominal cornering stiffness terms of the tires are perturbed by employing a sinusoidal function at frequency of 1 Hz and approximately 10 of the nominal magnitude. Other external disturbance sources related to a pulse-shaped function and random variations in the cornering stiffness at the longitudinal velocity of 20 m/s are further given in Table 4. The comparison of tracking performance under different disturbance conditions is presented in Table 5. It can be seen that the robustness of the proposed controller to withstand the effect of different disturbance functions is upheld and the performance of the proposed controller for the system subjected to external disturbances is on the verge of its unperturbed condition.

Table 4 Different external disturbances, in the longitudinal velocity 20m/s

Case 1:	Variation in c_f and c_r as $c_f = c_f + 5000 \sin(t)$
Case 2:	Variation in c_f and c_r as $c_f = c_f + 20,000[1 - 2 \times (\text{a random number between 0 and 1})]$
Case 3:	A pulse with width 0.1 at time 2.5 s

5.3 robustness against measurement errors

To show the robustness of the proposed control method against measurement errors, the simulations are carried out in this section for the vehicle traveling at 10 m/s of longitudinal velocity subjected to white noise with different variances to the measured in the states. The values of RMS and maximum of tracking errors for different noise levels are given in Table 6 and are compared with the use of type 1 fuzzy systems (T1FSs) in the control scheme. Table 6 shows that the increase in noise variance level invariably increases the path-following errors of the autonomous vehicle. However, it is evident that the proposed control scheme, by using the proposed non-singleton fuzzification, results in a high robust performance while it is subjected to the measurement errors. The performance of both control methods has not been degraded in terms of the heading angle error, and the measurement noise only affects the lateral offset error within a limited band. It must be noted that the effect of approximation errors is eliminated by the use of proposed adaptive compensator. Then in the normal condition, the tracking performance with the use of T1FS and proposed fuzzy system is almost equal.

6 Conclusion

The problem of path-following of autonomous vehicles as an arduous task of control design has gained a considerable attention because of the range of effective parameters and their variations at critical driving maneuvers. In this paper, a robust fuzzy control approach is proposed for the path-following control of autonomous vehicles by employing non-singleton fuzzy system and non-stationary fuzzy sets. Active front wheel steering (AFS) and direct yaw moment control (DYC) were employed as the control inputs of the closed-loop system, and the asymptotic stability of the proposed method is guaranteed based on the Lyapunov stability theorem. It is shown that the proposed approach holds the capacity to improve the transient performance, eliminates the steady-state errors in the path-following maneuver and withstands the effects arising from the system uncertainties and time-varying reference which is due to the variations in the forward speed. The effectiveness of the proposed control

Table 5 Comparison of RMS and maximum values of tracking error in the presence of different external disturbances

	Normal	Case 1	Case 2	Case 3
y	0.0638	0.0638	0.0639	0.0621
$\max(e_y)$	0.1198	0.1198	0.1200	0.1165
ψ	7.8899e-04	7.8879e-4	7.9045e-4	7.7564e-04
$\max(e_\psi)$	0.0018	0.0018	0.0018	0.0018

Table 6 Comparison of RMS and maximum values of tracking error in the presence of different measurement errors

Noise variance	Fuzzy system	y	$\max(e_y)$	ψ	$\max(e_\psi)$
0	T1FS	0.0269	0.0452	0.0010	0.0017
	Proposed FS	0.0268	0.0451	0.0010	0.0017
0.5	T1FS	0.0374	0.0632	0.0010	0.0018
	Proposed FS	0.0367	0.0609	0.0010	0.0018
1	Singleton	0.0700	0.1430	0.0010	0.0019
	Proposed FS	0.0683	0.1385	0.0010	0.0019

method is verified for a vehicle system performing a double-lane-change (DLC) maneuver at different forward speeds subjected to different disturbances related to uncertainty in the lateral force variations. Furthermore, the robustness of the proposed approach is evaluated under different measurement noise levels. Based on the obtained results, it is demonstrated that the proposed control strategy can be effectively applied for the path-following task of autonomous vehicles under a wide range of operating conditions and external disturbances. The most important disadvantage of proposed control scenario that can be considered in the future studies is that there is no constraint on the control signals.

Compliance with ethical standards

Conflict of interest The authors declare that they have no conflict of interest.

Ethical approval This article does not contain any studies with human participants or animals performed by any of the authors.

References

- Aguiar AP, Hespanha JP (2007) Trajectory-tracking and path-following of underactuated autonomous vehicles with parametric modeling uncertainty. *IEEE Trans Autom Control* 52(8):1362–1379
- Castillo O, Melin P, Alanis A, Montiel O, Sepúlveda R (2011) Optimization of interval type-2 fuzzy logic controllers using evolutionary algorithms. *Soft Comput* 15(6):1145–1160
- Deng Wu, Zhao Huimin, Yang Xinhua, Xiong Juxia, Sun Meng, Li Bo (2017) Study on an improved adaptive PSO algorithm for solving multi-objective gate assignment. *Appl Soft Comput* 59:288–302
- Deng Wu, Zhao Huimin, Zou Li, Li Guangyu, Yang Xinhua, Wu Daqing (2017) A novel collaborative optimization algorithm in solving complex optimization problems. *Soft Comput* 21(15):4387–4398
- Deng Wu, Zhang Shengjie, Zhao Huimin, Yang Xinhua (2018) A novel fault diagnosis method based on integrating empirical wavelet transform and fuzzy entropy for motor bearing. *IEEE Access* 6:35042–35056
- Deng Wu, Xu Junjie, Zhao Huimin (2019) An improved ant colony optimization algorithm based on hybrid strategies for scheduling problem. *IEEE Access* 7:20281–20292
- Deng Wu, Yao Rui, Zhao Huimin, Yang Xinhua, Li Guangyu (2019) A novel intelligent diagnosis method using optimal LS-SVM with improved PSO algorithm. *Soft Comput* 23(7):2445–2462
- Falcone P, Borrelli F, Asgari J, Tseng HE, Hrovat D (2007) Predictive active steering control for autonomous vehicle systems. *IEEE Trans Control Systems Technol* 15(3):566–580
- Fang H, Dou L, Chen J, Lenain R, Thuilot B, Martinet P (2011) Robust anti-sliding control of autonomous vehicles in presence of lateral disturbances. *Control Eng Pract* 19(5):468–478
- Garibaldi JM, Jaroszewski M, Musikasuwan S (2008) Nonstationary fuzzy sets. *IEEE Trans Fuzzy Syst* 16(4):1072–1086
- Ghaffari S, Homaeinezhad M (2018) Autonomous path following by fuzzy adaptive curvature-based point selection algorithm for four-wheel-steering car-like mobile robot. *Proc Inst Mech Eng Part C J Mech Eng Sci* 232(15):2655–2665
- González D, Pérez J, Milanés V, Nashashibi F (2016) A review of motion planning techniques for automated vehicles. *IEEE Trans Intell Transp Syst* 17(4):1135–1145
- Guo H, Song L, Liu J, Wang F-Y, Cao D, Chen H, Lv C, Luk PC-K (2018) Hazard-evaluation-oriented moving horizon parallel steering control for driver-automation collaboration during automated driving. *IEEE/CAA J Automat Sin* 5(6):1062–1073
- He W, Chen Y, Yin Z (2016) Adaptive neural network control of an uncertain robot with full-state constraints. *IEEE Trans Cybern* 46(3):620–629
- Hu W-RYFCC (2016) Output constraint control on path following of four-wheel independently actuated autonomous ground vehicles. *IEEE Trans Veh Technol* 65(6):4033–4043
- Hu C, Wang R, Yan F, Chen N (2015) Should the desired heading in path following of autonomous vehicles be the tangent direction of the desired path? *IEEE Trans Intell Transp Syst* 16(6):3084–3094
- Hu C, Wang R, Yan F, Karimi HR (2016) Robust composite nonlinear feedback path-following control for independently actuated autonomous vehicles with differential steering. *IEEE Trans Transp Electrif* 2(3):312–321
- Hu C, Wang R, Yan F (2016) Integral sliding mode-based composite nonlinear feedback control for path following of four-wheel

- independently actuated autonomous vehicles. *IEEE Trans Transp Electrif* 2(2):221–230
- Hu C, Qin Y, Cao H, Song X, Jiang K, Rath JJ, Wei C (2019) Lane keeping of autonomous vehicles based on differential steering with adaptive multivariable super-twisting control. *Mech Syst Signal Process* 125:330–346. <https://doi.org/10.1016/j.ymssp.2018.09.011>
- Hwang C-L, Yang C-C, Hung JY (2018) Path tracking of an autonomous ground vehicle with different payloads by hierarchical improved fuzzy dynamic sliding-mode control. *IEEE Trans Fuzzy Syst* 26(2):899–914
- Jeon D, Kim D-H, Ha Y-G, Tyan V (2016) Image processing acceleration for intelligent unmanned aerial vehicle on mobile gpu. *Soft Comput* 20(5):1713–1720
- Ji X, He X, Lv C, Liu Y, Wu J (2018) Adaptive-neural-network-based robust lateral motion control for autonomous vehicle at driving limits. *Control Eng Pract* 76:41–53
- Kang CM, Kim W, Chung CC (2018) Observer-based backstepping control method using reduced lateral dynamics for autonomous lane-keeping system. *ISA Trans* 83:214–226
- Li X, Sun Z, Cao D, Liu D, He H (2017) Development of a new integrated local trajectory planning and tracking control framework for autonomous ground vehicles. *Mech Syst Signal Process* 87:118–137
- Naranjo JE, Gonzalez C, Garcia R, De Pedro T (2008) Lane-change fuzzy control in autonomous vehicles for the overtaking maneuver. *IEEE Trans Intell Transp Syst* 9(3):438
- Rastelli JP, Peñas MS (2015) Fuzzy logic steering control of autonomous vehicles inside roundabouts. *Appl Soft Comput* 35:662–669
- Rodriguez-Castaño A, Heredia G, Ollero A (2016) High-speed autonomous navigation system for heavy vehicles. *Appl Soft Comput* 43:572–582
- Saffiotti A (1997) The uses of fuzzy logic in autonomous robot navigation. *Soft Comput* 1(4):180–197
- Shih C-C, Horng M-F, Pan T-S, Pan J-S, Chen C-Y (2017) A genetic-based effective approach to path-planning of autonomous underwater glider with upstream-current avoidance in variable oceans. *Soft Comput* 21(18):5369–5386
- Wai R-J, Liu C-M, Lin Y-W (2010) Robust path tracking control of mobile robot via dynamic petri recurrent fuzzy neural network. *Soft Comput* 15(4):743–767
- Wang R, Jing H, Hu C, Yan F, Chen N (2016) Robust H_∞ path following control for autonomous ground vehicles with delay and data dropout. *IEEE Trans Intell Transp Syst* 17(7):2042–2050
- Wang J, Wang J, Wang R, Hu C (2017) A framework of vehicle trajectory replanning in lane exchanging with considerations of driver characteristics. *IEEE Trans Veh Technol* 66(5):3583–3596
- Xia Y, Pu F, Li S, Gao Y (2016) Lateral path tracking control of autonomous land vehicle based on adrc and differential flatness. *IEEE Trans Ind Electron* 63(5):3091–3099
- Yang F, Yuan R, Yi J, Fan G, Tan X (2013) Direct adaptive type-2 fuzzy neural network control for a generic hypersonic flight vehicle. *Soft Comput* 17(11):2053–2064
- Yim S, Kim S, Yun H (2016) Coordinated control with electronic stability control and active front steering using the optimum yaw moment distribution under a lateral force constraint on the active front steering. *Proc Inst Mech Eng Part D J Automob Eng* 230(5):581–592
- Zhang C, Hu J, Qiu J, Yang W, Sun H, Chen Q (2019) A novel fuzzy observer-based steering control approach for path tracking in autonomous vehicles. *IEEE Trans Fuzzy Syst* 27:278–290. <https://doi.org/10.1109/TFUZZ.2018.2856187>
- Zhao Huimin, Sun Meng, Deng Wu, Yang Xinhua (2016) A new feature extraction method based on EEMD and multi-scale fuzzy entropy for motor bearing. *Entropy* 19(1):14
- Zhu M, Chen H, Xiong G (2017) A model predictive speed tracking control approach for autonomous ground vehicles. *Mech Syst Signal Process* 87:138–152

Publisher's Note Springer Nature remains neutral with regard to jurisdictional claims in published maps and institutional affiliations.